

Dark Matter Annual Modulation Analysis with Combined Nuclear and Electron Recoil Channels

H.B. Li,^{1,*} M.K. Pandey,^{2,†} C.H. Leung,¹ L. Singh,^{3,1} H.T. Wong,^{1,‡} H.-C. Chi,⁴ M. Deniz,^{5,1} Greeshma C.,^{1,3} J.-W. Chen,² H.C. Hsu,¹ S. Karadağ,^{1,6} S. Karmakar,^{1,7} V. Kumar,^{1,7} J. Li,⁸ F.K. Lin,¹ S.T. Lin,^{9,1} C.-P. Liu,⁴ S.K. Liu,⁹ H. Ma,⁸ D.K. Mishra,^{3,1} K. Saraswat,¹ V. Sharma,^{10,1} M.K. Singh,^{1,11} M.K. Singh,^{7,1} V. Singh,^{3,11,1} D. Tanabe,¹ J.S. Wang,¹ C.-P. Wu,^{2,4} L.T. Yang,⁸ C.H. Yeh,¹ and Q. Yue⁸

(TEXONO Collaboration)

¹*Institute of Physics, Academia Sinica, Taipei 11529.*

²*Department of Physics, CTP and LeCosPA, National Taiwan University, Taipei 10617.*

³*Department of Physics, School of Physical and Chemical Sciences, Central University of South Bihar, Gaya 824236.*

⁴*Department of Physics, National Dong Hwa University, Shoufeng, Hualien 97401.*

⁵*Department of Physics, Dokuz Eylül University, Buca, Izmir 35160.*

⁶*Department of Physics Engineering, Istanbul Technical University, Sariyer, Istanbul 34467.*

⁷*Department of Physics, Institute of Applied Sciences and Humanities, GLA University, Mathura 281406.*

⁸*Department of Engineering Physics, Tsinghua University, Beijing 100084.*

⁹*College of Physics, Sichuan University, Chengdu 610065.*

¹⁰*Department of Physics, H.N.B. Garhwal University, Srinagar, Uttarakhand 246174.*

¹¹*Department of Physics, Institute of Science, Banaras Hindu University, Varanasi 221005.*

(Dated: December 9, 2024)

After decades of experimental efforts, the DAMA/LIBRA(DL) annual modulation (AM) analysis on the χN (WIMP Dark Matter interactions on nucleus) channel remains the only one which can be interpreted as positive signatures. This has been refuted by numerous time-integrated (TI) and AM analysis. It has been shown that χe (WIMP interactions with electrons) alone is not compatible with the DL AM data. We expand the investigations by performing an AM analysis with the addition of χe long-range and short-range interactions to χN , derived using the frozen-core approximation method. Two scenarios are considered, where the χN and χe processes are due to a single χ ($\Gamma_{tot}^{1\chi}$) or two different χ 's ($\Gamma_{tot}^{2\chi}$). The combined fits with χN and χe provide stronger significance to the DL AM data which are compatible with the presence of additional physical effects beyond χN alone. This is the first analysis which explores how χe AM can play a role in DL AM. The revised allowed regions as well as the exclusion contours from the other null AM experiments are presented. All DL AM allowed parameter spaces in χN and χe channels under both $\Gamma_{tot}^{1\chi}$ and $\Gamma_{tot}^{2\chi}$ are excluded at the 90% confidence level by the combined null AM results. It can be projected that DL-allowed parameter spaces from generic models with interactions induced by two-WIMPs are ruled out.

There are compelling experimental evidence that about one-quarter of the energy density of the Universe is composed of dark matter (DM), whose exact nature and properties remain unknown. Searches of DM in numerous directions with diverse techniques are intense areas of fundamental research [1]. A favored DM candidate is the weakly interacting massive particle (WIMP, denoted as χ) [2, 3]. Direct experimental searches assume finite interactions between WIMPs with electrons (χe) and nuclei (χN). Positive signatures manifest as excess events over known background in the measured “time-integrated” (TI) energy spectra and in their annual modulation (AM) due to changes of the relative velocity between Earth and the WIMPs in the galactic halo [4]. TI analysis is sensitive to uncertainties of background modeling while AM analysis only requires the background is stable with time but independent of other details.

After decades of experimental efforts, the only result consistent with positive WIMP signatures is from the AM analysis on χN from the DAMA/LIBRA(DL) experiment with NaI(Tl) scintillating crystals [5]. This interpretation, however, is challenged and rejected by numerous

χN experiments with TI analysis [1] and several with AM analysis [6–10] using a variety of targets. There are attempts to explain the DL AM data with scenarios other than χN detection, such as complications in the analysis procedures [11, 12]. In addition, it has been shown [13] – and verified in our studies – that AM analysis with the χe -channels only (setting $\sigma_{\chi N}^{SI}=0$ in Eq. 1) is unable to provide an acceptable fit to the DL data. The maximum electron recoil energy even for infinite m_χ is about 3 keV_{ee}, in serious discrepancy with the data.

We performed an analysis including *both* χe and χN interactions. The combined analysis would provide better matching statistically to the DL data. Three types of WIMPs interactions are included: spin-independent WIMP-nucleon interaction (χN^{SI}), long and short-range WIMP-electron interaction (χe^{LR} and χe^{SR} , respectively) [16]. Their cross-sections (respectively $\sigma_{\chi N}^{SI}$, $\sigma_{\chi e}^{LR}$ and $\sigma_{\chi e}^{SR}$) are all functions of m_χ . The input to the analysis, as depicted in Figure 1a, are the published AM amplitude data from these experiments: DL [14], CO-SINE [9] and ANAIS [10, 15] with NaI(Tl), XMASS with Xe [6] and CDEX with Ge [7]. These AM data sets are

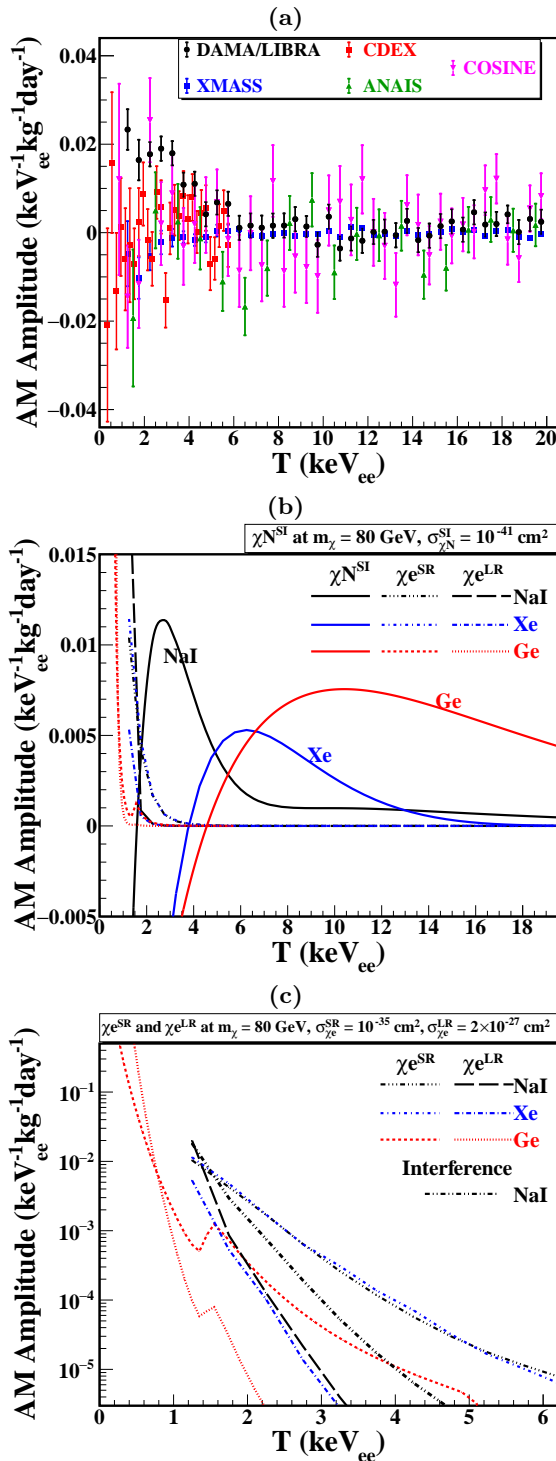


FIG. 1. (a) Published AM amplitudes data from DM experiments with NaI in DL [14], COSINE [9] and ANAIS [10, 15], Xe in XMASS [6] and Ge in CDEX [7]. For display purposes, the depicted event rates are re-scaled to account for the differences in bin-sizes and target mass number squared. The expected differential AM spectra for positive WIMP signatures in: (b) $\chi^{N^{SI}}$ and (c) in $\chi^{e^{LR}}$ and $\chi^{e^{SR}}$ for all three targets taking the case of $m_\chi = 80$ GeV as example, together with the interference spectrum between $\chi^{e^{LR}}$ and $\chi^{e^{SR}}$ for NaI. The $\chi^{e^{LR}}$ and $\chi^{e^{SR}}$ spectra in (c) are superimposed as dotted lines in (b) f showing their responses to AM are very different from $\chi^{N^{SI}}$. The interference spectrum between $\chi^{e^{LR}}$ and $\chi^{e^{SR}}$ for NaI is also displayed in (c).

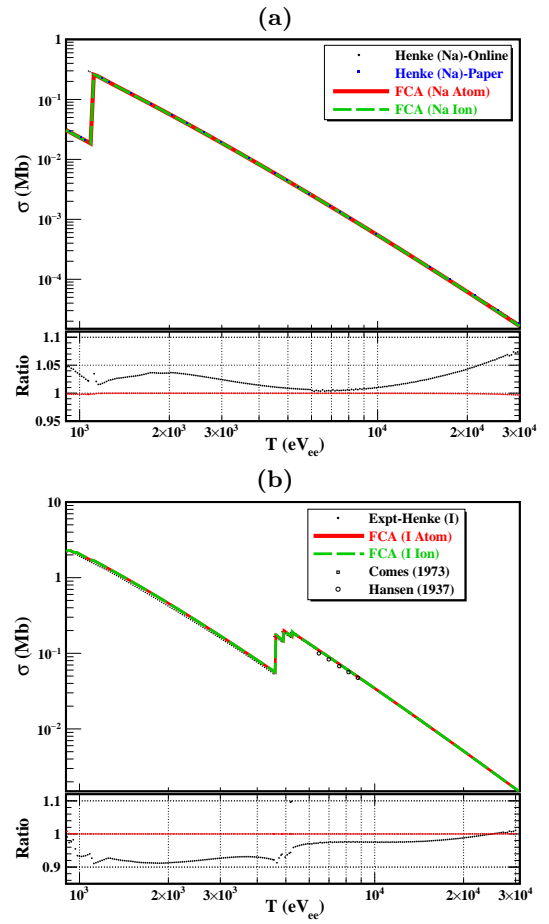


FIG. 2. Photo-ionization cross-sections derived by FCA following Ref. [16] for (a) Na and (b) I, both as atoms and ions, within 1 keV_{ee} to 30 keV_{ee} energy transfer, The experimental data [17] and theoretical values [18, 19] are superimposed. Relative deviations from benchmark data are displayed.

complementary in their strength in probing different parameter space. COSINE and ANAIS use the same detector technology with identical target isotopes as DL. Comparisons would be model-independent in principle, though the variations on quenching factors among different NaI(Tl) crystals have been raised [20]. CDEX is distinguished with low detector threshold (0.16 keV_{ee}) while XMASS has big exposure (1.82 ton-year). The electron-equivalent unit keV_{ee} is used to characterize detector response and measured energy (T), unless otherwise stated.

The maximum(minimum) AM amplitude are on June 1(December 2) [21, 22] following the standard DM halo model [1, 4]. The quenching factors used by DL [23] is applied to all the three NaI(Tl) experiments. The expected AM differential spectra for positive WIMP signatures in $\chi^{N^{SI}}$ for the three targets are displayed in Figure 1b. The AM shapes originate from the differences in χ -velocity relative to Earth between summer and winter. A characteristic feature is a drop from enhancement to deficit at

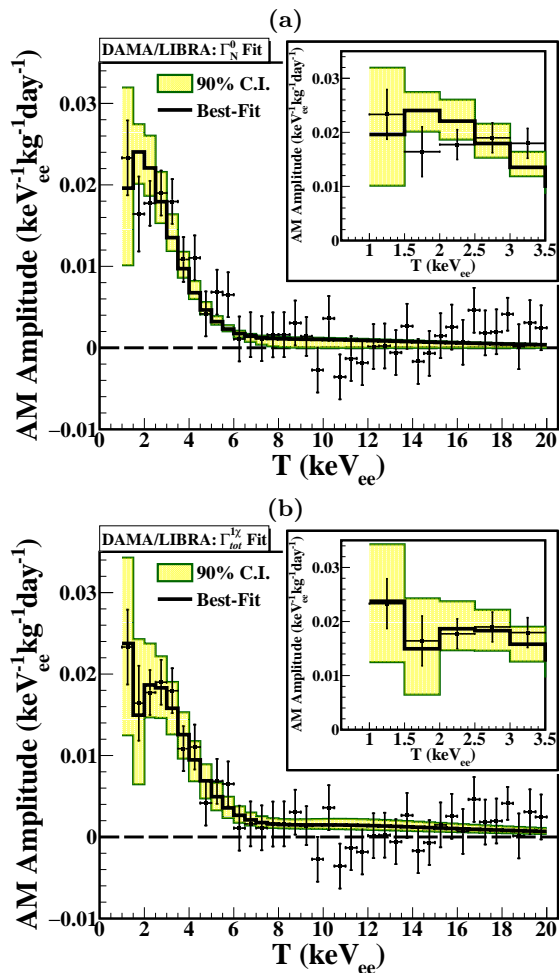


FIG. 3. DL data [14] with best-fits under (a) Γ_N^0 : with χN only where $m_\chi=54$ GeV, and (b) $\Gamma_{tot}^{1\chi}$: with all three channels (χN^{SI} , χe^{LR} , χe^{SR}) combined, in which case $m_\chi=83$ GeV.

low energy. The turning point is m_χ -dependent.

Recent interest in the searches of light dark matter brings along intense activities in exploring novel detector concepts. Crucial to this development is the χe detection channels which triggers intense research efforts in the refinement on the evaluation of its interactions with atoms A in $\chi+A \rightarrow \chi+e^-+A^+$ [16, 24]. Following our previous work on Ge and Xe with the many body approach with conventional frozen-core approximation (FCA) [16, 25, 26], we use same approach for Na and I prescribed in Ref. [16] in this analysis. The results are validated by comparing the derived photo-ionization cross-sections against experimental data [17] and previous calculations [18, 19]. The photo-ionization cross-sections of Na and I are illustrated in Figures 2a&b, showing consistency of theory calculations with measured data to within 5% across the entire energy transfer range. Identical results are obtained whether the targets are treated as atoms or ions. The differential AM spectra

in χe^{LR} and χe^{SR} for the three target nuclei are shown in Figure 1c. The χe recoil energy is shifted lower in winter, giving rise to rapidly rising AM spectra. The long-range χe interactions has an additional $1/q^2$ term where q is the 3-momentum transfer [16]. The differential AM spectra therefore rise steeper at low recoil energy such that studies of χe^{LR} favor experiments with lower detection threshold. The AM spectra in χe^{LR} and χe^{SR} for NaI are superimposed to the χN^{SI} spectra in Figure 1b, showing their vastly different response at low energy.

The best-fit estimators of the various cross-sections are derived by a minimum- χ^2 analysis. At a given m_χ ,

$$\chi^2 = \sum_i \frac{1}{\Delta_i^2} \left\{ n_i - \left[\sigma_{\chi N}^{SI} \phi_{\chi N}^{SI}(T_i) + \sigma_{\chi e}^{LR} \phi_{\chi e}^{LR}(T_i) + \sigma_{\chi e}^{SR} \phi_{\chi e}^{SR}(T_i) + 2\sqrt{\sigma_{\chi e}^{LR}\sigma_{\chi e}^{SR}} \phi_{\chi e}^{int}(T_i) \right] \right\}^2 \quad (1)$$

where n_i and Δ_i are the AM amplitudes and uncertainties at the i^{th} -bin of average energy T_i , while $\phi_{\chi e}^{SI}$, $\phi_{\chi e}^{LR}$, $\phi_{\chi e}^{SR}$ are the normalized spectral functions for the three interactions. The interference spectrum ($\phi_{\chi e}^{int}$) between χe^{LR} and χe^{SR} follows the many-body χ -atom calculations given in Eq. 3 of Ref. [16], also depicted in Figure 1c.

The DL data shows positive AM signatures and reject the null hypothesis with large statistical significance. Its best-fit spectra with χN -channel only (Γ_N^0 : setting $\sigma_{\chi e}^{LR}=\sigma_{\chi e}^{SR}=0$ in Eq. 1) is displayed in Figure 3a. This analysis expands to have all three channels taken as the free fitting variables. Two DM scenarios are considered, parametrized by f_χ as the DM relic density fraction from the χ interacting via χe : (1) $\Gamma_{tot}^{1\chi}$ – Both χN and χe interactions are due to a single χ ($f_\chi=1$), such that same constraints on m_χ apply to all channels; (2) $\Gamma_{tot}^{2\chi}$ – The case of independent constraints where two different χ 's with fractional density f_χ and $(1-f_\chi)$ interact separately via χe and χN , respectively. The limiting case of $f_\chi=0$ corresponds to the baseline Γ_N^0 . The analysis of $\Gamma_{tot}^{2\chi}$ is applicable to generic interactions by two independent WIMPs.

The combined best-fit in $\Gamma_{tot}^{1\chi}$ is given in Figure 3b. The allowed bands of $\sigma_{\chi N}^{SI}$ are derived with the Wilks' Approximation [27]. It can be seen that the addition of the χe -channels provides better description of the AM data at low energy near threshold, and the $\Gamma_{tot}^{1\chi}$ -fit is a more inclusive and general form than the conventional Γ_N^0 . As illustrated in Table I, the analysis reveal that the interpretation of the DL data incorporating $\Gamma_{tot}^{1\chi}$ or $\Gamma_{tot}^{2\chi}$ has higher statistical significance than Γ_N^0 alone. The low energy data (1–4 keV_{ee}) gives a p-values of 0.52 for $\Gamma_{tot}^{(1\chi,2\chi)}$ but only 0.07 for Γ_N^0 , indicating that the χN^{SI} channel as the sole physics scenario cannot explain the low energy data. In addition, the differences in χ^2/dof between Γ_N^0 and $\Gamma_{tot}^{(1\chi,2\chi)}$ (7.26/2 for $T=1-4$ keV_{ee} and 9.66/2 for $T=1-20$ keV_{ee}) correspond to p-values of 0.02

	$\Gamma_N^0:$ χN^{SI}	$\Gamma_{tot}^{(1\chi,2\chi)}:$ $\chi N^{SI} + \chi e^{LR} + \chi e^{SR}$	Compare
Data (keV _{ee})		χ^2/dof (p-value)	$\Delta\chi^2/\text{dof}$ (p-value)
1 - 20	32.06/36 (0.66)	22.40/34 (0.94)	9.66/2 (0.008)
1 - 4	8.6/4 (0.07)	1.3/2 (0.52)	7.26/2 (0.02)

TABLE I. Comparison of statistical significance (as χ^2/dof and p-values) in the Γ_N^0 and $\Gamma_{tot}^{(1\chi,2\chi)}$ fits to the DL AM data [14]. The increased significance from 1 to 3 fitting parameters indicates the presence of additional physical processes.

and 0.008, respectively. This implies the necessity of having additional physical processes such as χe^{LR} and χe^{SR} to explain the AM spectrum [28].

On the contrary, no AM signatures were observed in the COSINE, ANAIS, XMASS, CDEX experiments. Their data are consistent with the null hypothesis. Conservative and inclusive limits are derived with single-channel (Γ_N^0) analysis – $\sigma_{\chi e}^{LR}$ and $\sigma_{\chi e}^{SR}$ are set to be zero in Eq. 1 while the best-fit values of $\sigma_{\chi N}^{SI}$ are evaluated, allowing negative values. Limits are derived with the unified approach [29]. Same procedures apply for $\sigma_{\chi e}^{LR}$ and $\sigma_{\chi e}^{SR}$ by assuming two other σ 's are zero.

The allowed regions in both $\pm 3\sigma$ and 90% confidence intervals (C.I.) for χN^{SI} , χe^{LR} and χe^{SR} as functions of m_χ under $\Gamma_{tot}^{1\chi}$ -analysis from DL AM data [14] are shown, respectively, in Figures 4a,b&c. The exclusion contours showing upper limits at 90% confidence level (C.L.) from the null AM experiments are superimposed for comparisons in the same plots. Results of Γ_N^0 are superimposed in Figure 4a for comparison. The relevant ranges of the Earth attenuation and scattering effects correspond to much higher cross-sections and the bounds are outside to the plots displayed. For instance for the CDEX experiment at 2.4 km of rock overburden, the upper limits of the sensitivity regions are 10^{-30} cm² for $\sigma_{\chi N}^{SI}$ [30], 10^{-24} cm² for $\sigma_{\chi e}^{LR}$, and 10^{-29} cm² for $\sigma_{\chi e}^{SR}$.

There are two allowed regions in Γ_N^0 at 90% C.I. at low and high m_χ corresponding to Na and I-recoils, respectively. With χe^{LR} and χe^{SR} are added in $\Gamma_{tot}^{1\chi}$, only the high m_χ region due to I-recoils is allowed at the same significance. The best-fit solution of m_χ is shifted from (54.25 ± 4.25) GeV in Γ_N^0 to (83.3 ± 25.65) GeV in $\Gamma_{tot}^{1\chi}$. The χe -channels dominate the near-threshold behavior, while the high energy (>3 keV_{ee}) spectra are defined by χN . The two χe channels are highly correlated and share the strength of the AM counts at low energy. The limiting cases of the best-fit values in $\Gamma_{tot}^{1\chi}$ of $\sigma_{\chi e}^{LR}$ at $\sigma_{\chi e}^{SR}=0$ and $\sigma_{\chi e}^{SR}$ at $\sigma_{\chi e}^{LR}=0$ correspond to the red circles in Figures 4b&c, respectively. The exclusion contours of the null AM experiments are superimposed. The weaker

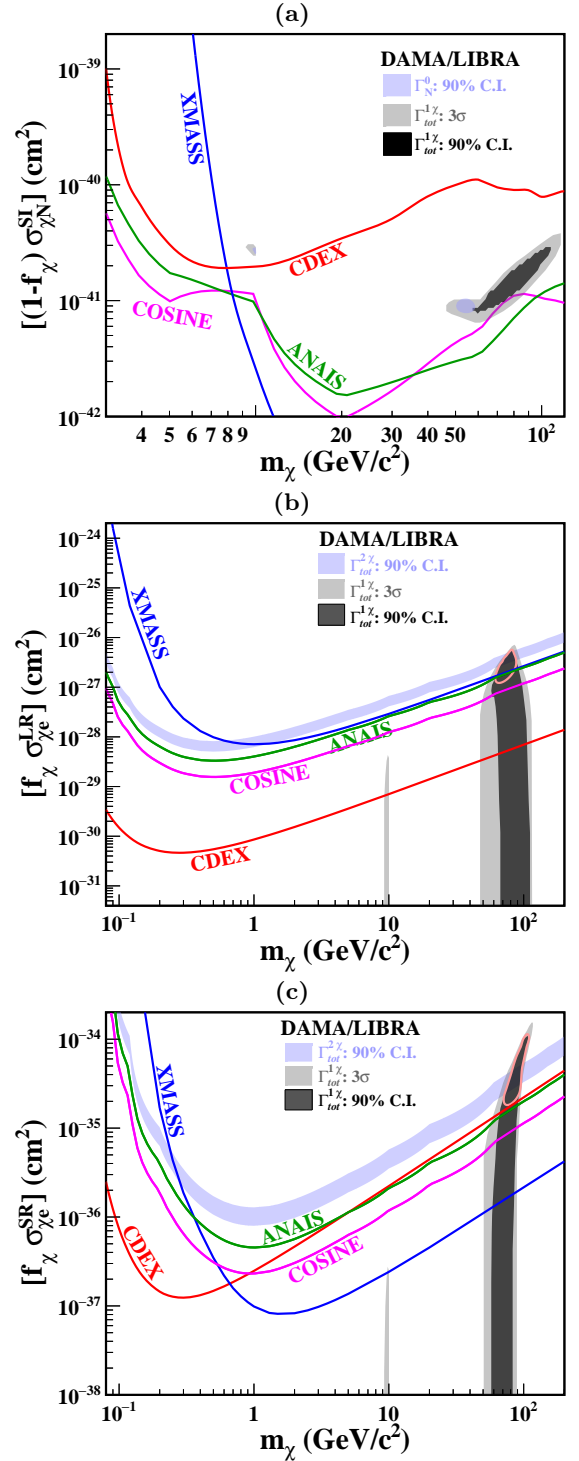


FIG. 4. Exclusion Plots with AM Data from Na+I, Ge and Xe experiments with (a) $\sigma_{\chi N}^{SI}$ (b) $\sigma_{\chi e}^{LR}$, and (c) $\sigma_{\chi e}^{SR}$ versus m_χ . Y-axes are presented in $[f_\chi \sigma]$ to accommodate both scenarios $\Gamma_{tot}^{1\chi}$ ($f_\chi=1$) and $\Gamma_{tot}^{2\chi}$ ($0 < f_\chi < 1$). The DL allowed regions [14] from $\Gamma_{tot}^{1\chi}$ at 90% ($\pm 3\sigma$) C.I. are presented as dark(light) shaded areas. The case of Γ_N^0 is included in (a) as comparison. Exclusion contours from the null AM experiments represent upper limits at 90% C.L. Red circles of (b,c) are 90% allowed regions from $\Gamma_{tot}^{1\chi}$ for ($\sigma_{\chi e}^{LR}$ at $\chi e^{SR}=0, \sigma_{\chi e}^{SR}$ at $\sigma_{\chi e}^{LR}=0$) while the blue bands correspond to those from $\Gamma_{tot}^{2\chi}$.

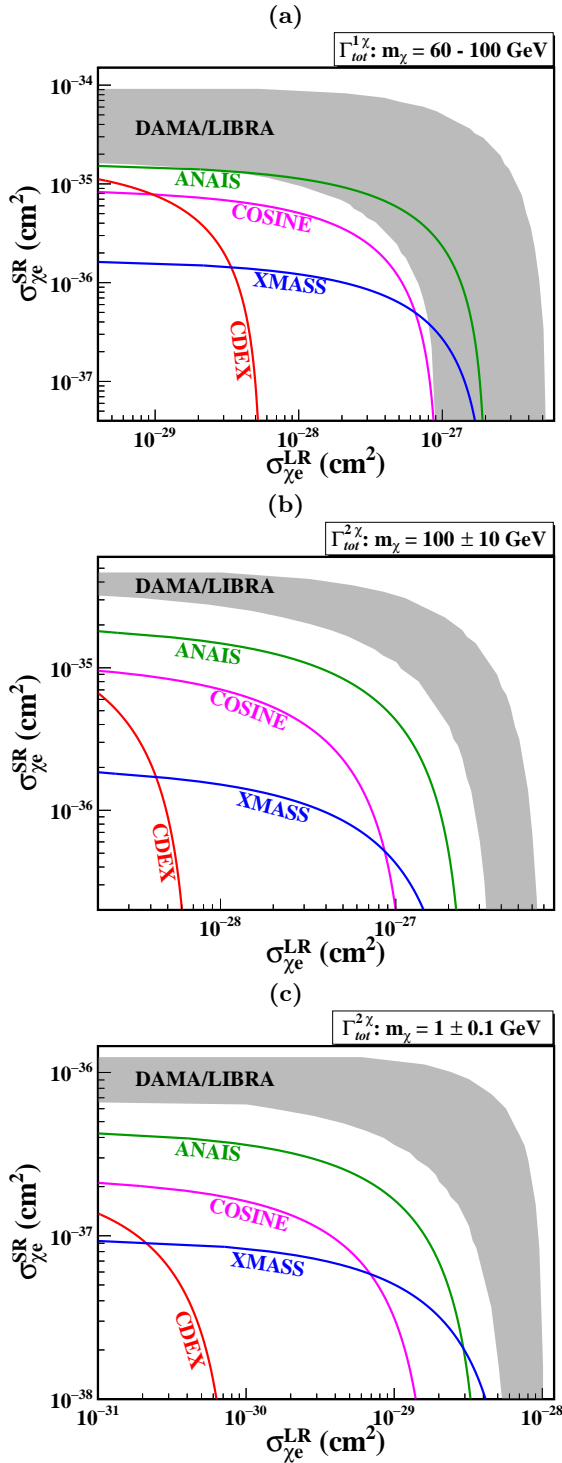


FIG. 5. Correlations between $\sigma_{\chi e}^{\text{SR}}$ and $\sigma_{\chi e}^{\text{LR}}$, showing the allowed region in the 90% C.I. from DL AM data [14] and in comparison with the null AM experiments at upper limits at 90% C.L. (a) with the $\Gamma_{\text{tot}}^{1\chi}$ analysis, where the best-fit m_χ -range is (60-100) GeV, and with the $\Gamma_{\text{tot}}^{2\chi}$ analysis, at (b) $m_\chi=(100\pm 10)$ GeV, and (c) $m_\chi=(1\pm 0.1)$ GeV.

bounds in $\sigma_{\chi e}^{\text{LR}}$ in Figure 4b originates from its sharper rise of the AM spectra due to an additional $(1/q^2)$ dependence, so that only the low threshold data from CDEX places strong constraints. Under $\Gamma_{\text{tot}}^{1\chi}$, the DL AM allowed regions in Figures 4a,b&c are inter-dependent – m_χ is constrained to (60-100) GeV by the χN^{SI} channel. The correlations of $(\sigma_{\chi e}^{\text{LR}}, \sigma_{\chi e}^{\text{SR}})$ in this m_χ range are depicted in Figure 5a, showing the DL allowed region in $\Gamma_{\text{tot}}^{1\chi}$ is excluded by the null AM experiments, and in particular with large margins by CDEX and XMASS combined.

In the scenario of $\Gamma_{\text{tot}}^{2\chi}$ where χN and χe interactions are due to two different χ 's, the constraints due to the high and low energy AM spectral components are independent. The DL χN^{SI} allowed regions are defined by the high-energy component and remain those of Figure 4a, which are well-excluded by the other null experiments. The AM low-energy component is dominated by the χe channels of a different χ unconstrained in m_χ . This gives rise to allowed regions in $\Gamma_{\text{tot}}^{2\chi}$ represented by the blue bands in Figures 4b&c for $\sigma_{\chi e}^{\text{LR}}$ and $\sigma_{\chi e}^{\text{SR}}$, respectively. As illustration, the DL 90% allowed C.I. for $m_\chi=(100\pm 10)$ and (1 ± 0.1) GeV are depicted in Figure 5b&c, respectively, superimposed with the exclusion contours of the null AM data. It can be concluded that in the $\Gamma_{\text{tot}}^{2\chi}$ analysis, the DL AM allowed regions associated with χe are probed and rejected by the various null AM experiments. The CDEX [7] data placed more severe constraints on $\sigma_{\chi e}^{\text{LR}}$ where the $(1/q^2)$ dependence favors low threshold experiments. The XMASS [6] experiment is more sensitive to $\sigma_{\chi e}^{\text{SR}}$ due to its large exposure. It can be projected from the results that the DL allowed regions in generic two-WIMP models are ruled out by the null AM experiments. Very little room is left to account for the DL AM data with WIMP-induced effects.

This work is supported by contracts 106-2923-M-001-006-MY5, 110-2112-M-001-029-MY3, and 113-2112-M-001-053-MY3 from the National Science and Technology Council, Taiwan, grants 2021-22/TG2.1 from the National Center of Theoretical Sciences, Taiwan.

* Corresponding Author: lihb@gate.sinica.edu.tw

† Corresponding Author: pandey2148@g.ntu.edu.tw

‡ Corresponding Author: htwang@phys.sinica.edu.tw

- [1] P. A. Zyla *et al.* (Particle Data Group), Review of particle physics, *Progress of Theoretical and Experimental Physics* **2020**, 083C01 (2020).
- [2] H. Nilles, Supersymmetry, supergravity and particle physics, *Physics Reports* **110**, 1 (1984).
- [3] M. E. Peskin, Supersymmetric dark matter in the harsh light of the large hadron collider, *Proceedings of the National Academy of Sciences* **112**, 12256 (2015).
- [4] A. K. Drukier, K. Freese, and D. N. Spergel, Detecting cold dark-matter candidates, *Phys. Rev. D* **33**, 3495 (1986).
- [5] R. Bernabei *et al.*, The dama/libra apparatus, *Nuclear*

Instruments and Methods in Physics Research Section A: Accelerators, Spectrometers, Detectors and Associated Equipment **592**, 297 (2008).

- [6] K. Abe *et al.* (XMASS Collaboration 3), Direct dark matter search by annual modulation with 2.7 years of xmass-i data, *Phys. Rev. D* **97**, 102006 (2018).
- [7] L. T. Yang *et al.* (CDEX Collaboration), Search for light weakly-interacting-massive-particle dark matter by annual modulation analysis with a point-contact germanium detector at the china jinping underground laboratory, *Phys. Rev. Lett.* **123**, 221301 (2019).
- [8] J. Amaré *et al.*, Annual modulation results from three-year exposure of anais-112, .
- [9] N. Carlin *et al.*, Cosine-100 full dataset challenges the annual modulation signal of dama/libra (2024), [arXiv:2409.13226 \[hep-ex\]](https://arxiv.org/abs/2409.13226).
- [10] I. Coarasa *et al.*, Anais-112: updated results on annual modulation with three-year exposure (2023), [arXiv:2311.03392 \[astro-ph.IM\]](https://arxiv.org/abs/2311.03392).
- [11] G. Adhikari *et al.* (The COSINE-100 Collaboration), An experiment to search for dark-matter interactions using sodium iodide detectors, *Nature* **564**, 82 (2018).
- [12] D. Buttazzo *et al.*, Annual modulations from secular variations: relaxing dama?, *Journal of High Energy Physics* **2020**, [https://doi.org/10.1007/JHEP04\(2020\)137](https://doi.org/10.1007/JHEP04(2020)137) (2020).
- [13] B. M. Roberts and V. V. Flambaum, Electron-interacting dark matter: Implications from dama/libra-phase2 and prospects for liquid xenon detectors and nai detectors, *Phys. Rev. D* **100**, 063017 (2019).
- [14] R. Bernabei, , *et al.*, Improved model-dependent corollary analyses after the first six annual cycles of dama/libra-phase2, *Nuclear Physics and Atomic Energy* **20**, 317–348 (2019).
- [15] I. Coarasa Casas, *ANAIS-112. Searching for the annual modulation of dark matter with a 112.5 kg NaI(Tl) detector at the Canfranc Underground Laboratory.*, Ph.D. thesis, Zaragoza U. (2021).
- [16] M. K. Pandey *et al.*, Constraints from a many-body method on spin-independent dark matter scattering off electrons using data from germanium and xenon detectors, *Phys. Rev. D* **102**, 123025 (2020).
- [17] B. L. Henke, E. M. Gullikson, and J. C. Davis, X-Ray Interactions: Photoabsorption, Scattering, Transmission, and Reflection at $E = 50\text{-}30,000$ eV, $Z = 1\text{-}92$, *Atom. Data Nucl. Data Tabl.* **54**, 181 (1993).
- [18] H. Hansen, Die schwachung monochromatischer rontgenstrahlen in fliissigem, *Ann. Physik* **35**, 524 (1939).
- [19] F. J. Comes, U. Nielson, and W. H. E. Schwarz, Inner electron excitation of iodine in the gaseous and solid phase, *J. Chem. Phys.* **58**, 2230 (1973).
- [20] Y. Ko *et al.* (COSINE-100 Collaboration), Comparison between dama/libra and cosine-100 in the light of quenching factors, *Journal of Cosmology and Astroparticle Physics* **2019** (11), 008.
- [21] R. Bernabei *et al.*, First results from dama/libra and the combined results with dama/nai, *Eur. Phys. J. C* **56**, 333 (2008).
- [22] F. Froberg and A. R. Duffy, Annual modulation in direct dark matter searches, *Journal of Physics G: Nuclear and Particle Physics* **47**, 094002 (2020).
- [23] R. Bernabei *et al.*, New limits on wimp search with large-mass low-radioactivity nai(tl) set-up at gran sasso, *Physics Letters B* **389**, 757 (1996).
- [24] C.-P. Liu *et al.*, Spin-dependent dark matter-electron interactions, *Phys. Rev. D* **106**, 063003 (2022).
- [25] J. C. Slater, A simplification of the hartree-fock method, *Phys. Rev.* **81**, 385 (1951).
- [26] D. H. Sampson, H. L. Zhang, A. K. Mohanty, and R. E. H. Clark, A dirac-fock-slater approach to atomic structure for highly charged ions, *Phys. Rev. A* **40**, 604 (1989).
- [27] S. Algeri *et al.*, Searching for new phenomena with profile likelihood ratio tests, *Nature Reviews Physics* **2**, 245–252 (2020).
- [28] C. Werner and K. Schermelleh-Engel, Deciding between competing models: Chi-square difference tests, (2010).
- [29] G. J. Feldman and R. D. Cousins, Unified approach to the classical statistical analysis of small signals, *Phys. Rev. D* **57**, 3873 (1998).
- [30] Z. Z. Liu *et al.* (CDEX), Studies of the Earth shielding effect to direct dark matter searches at the China Jinping Underground Laboratory, *Phys. Rev. D* **105**, 052005 (2022), [arXiv:2111.11243 \[hep-ex\]](https://arxiv.org/abs/2111.11243).